Three-dimensional effects in directional solidification in Hele-Shaw cells: Nonlinear evolution and pattern selection

V. S. Ajaev and S. H. Davis
Department of Engineering Sciences and Applied Mathematics, Northwestern University, Evanston, Illinois 60208
(Received 18 June 1999)

Directional solidification of a dilute binary alloy in a Hele-Shaw cell is modeled by a long-wave nonlinear evolution equation with zero flux and contact-angle conditions at the walls. The basic steady-state solution and its linear stability criteria are found analytically, and the nonlinear system is solved numerically. Concave-down (toward the solid) interfaces under physically realistic conditions are found to be more unstable than the planar front. Weakly nonlinear analysis indicates that subcritical bifurcation is promoted, the domain of modulational instability is expanded and transition to three-dimensional patterns is delayed due to the contact-angle condition. In the strongly nonlinear regime fully three-dimensional steady-state solutions are found whose characteristic amplitude is larger than that for the two-dimensional problem. In the subcritical regime secondary bifurcation to stable solutions is promoted.

PACS number(s): 05.45.−a, 45.70.Qj, 47.20.Hw, 81.10.−h

I. INTRODUCTION

Directional solidification of binary alloys leads to a variety of interesting nonlinear phenomena, which have been studied analytically, numerically, and experimentally (see [1] for a review). Most theoretical models for nonlinear evolution in directionally solidified systems are two-dimensional; experiments, however, are usually carried out in Hele-Shaw cells, where three-dimensional effects can be important [2]. In particular, in steady state the interface can be curved, rather than planar, due to heat loses at the walls [3] or the boundary conditions at the line of contact between the solid-liquid interface and the wall. The influence of contact-line conditions has been studied for both symmetric [4] and one-sided [5] models.

Corrections to the classical linear stability criteria due to contact-angle effects were found analytically and verified numerically in [5]. Two different cases were considered in this study. First, the thickness was assumed to be small enough so that no instability wavelength can fit into the gap between the plates. Correction to the stability criterion is found to be small under physically realistic conditions. The second case discussed involves values of thickness near the one-half of the Mullins-Sekerka wavelength. It is referred to as ''resonant'' since the behavior of the system here is determined by the interactions between the growing disturbance and the leading Fourier mode of the basic-state solution. Stability criteria can differ significantly from those for the planar interface.

The approach taken in [5] does not allow one to describe nonlinear evolution of the front for arbitrary values of gap width or far away from the initial bifurcation point. In order to obtain such description and study pattern formation some simplified model equations are needed. A natural simplification of the problem is achieved by using long-wave evolution equations. In this approach the full system of equations and boundary conditions for directional solidification is reduced to a single partial differential equation. This has been carried out for small values of segregation coefficient in constitutional supercooling regime [6] and for the large surface energy [7]. For arbitrary values of segregation coefficient a long-wave evolution equation has been obtained near the absolute stability limit [8]. All these equations were derived for the infinite domain, which is usually modeled numerically by periodic boundary conditions. In the present study similar ideas will be used for solidification in Hele-Shaw cells with contact-angle and no-flux conditions at the walls. The resulting system is solved numerically to show how even in Hele-Shaw cells three-dimensional evolution emerges.

II. FORMULATION

Consider directional solidification at constant speed V of a dilute binary alloy in a Hele-Shaw cell as shown in Fig. 1. The solute diffusivity in the liquid phase D_L is usually much larger than that in the solid phase, and so diffusion in the solid is neglected. The ''frozen temperature approximation'' is used [1], which implies equal thermal conductivities in solid and liquid, negligible latent heat release in the interfacial heat balance, and large thermal diffusion length. With these assumptions the value of thermal gradient G_T is the same in both phases; the temperature profile is hence linear.

Scale the independent variables as follows: length by the concentration-boundary-layer thickness $\delta_c = D_L/V$ and time by δ_c/V. The nondimensional governing equation and boundary conditions at the solid-liquid interface are the following:

$$C_t - C_z = \nabla^2 C, \quad z > h(x,y,t), \tag{1}$$

$$[C(k-1)+1](1+h_t) = \mathbf{n}\cdot\nabla C, \quad z = h(x,y,t), \tag{2}$$

$$M^{-1}h = C + \Gamma\mathcal{K}(h), \quad z = h(x,y,t). \tag{3}$$

Here the reference frame moves with speed V so that x and y are along the interface, parallel to and normal to the walls, respectively, and z is oriented along the pulling direction, as shown in Fig. 1, $\mathbf{n} = (-h_x, -h_y, 1)$ is a normal vector to the interface $z = h(x,y,t)$ pointing into the liquid. The morphological number M and the surface-tension parameter Γ are defined as follows:

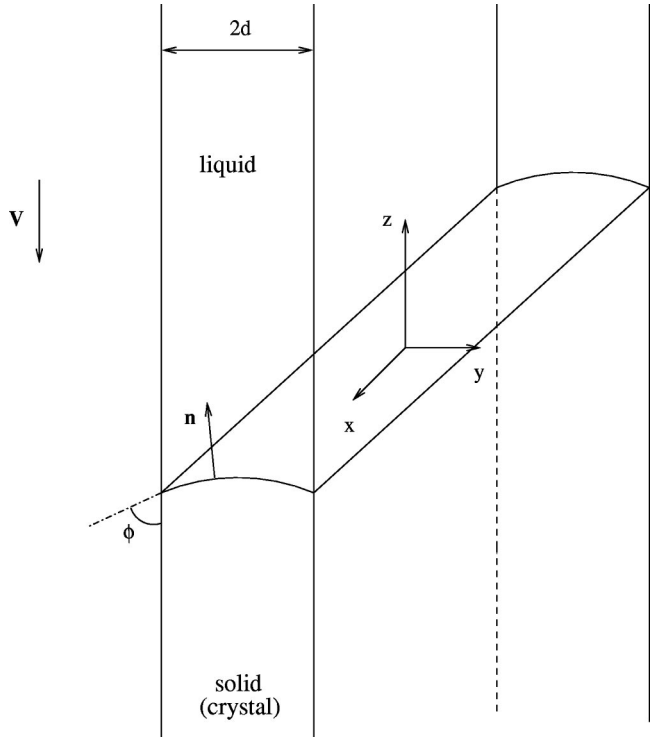

FIG. 1. Experimental configuration and coordinate system for directional solidification in a Hele-Shaw cell. The angle ϕ between the solid-liquid interface and the wall is different from $\pi/2$, so the steady-state solution is a curved front.

$$M=\frac{mc_\infty(k-1)}{G_T k\delta_c},\quad \Gamma=\frac{\gamma T_M k}{L_v m\delta_c c_\infty(k-1)}.$$

Here c_∞ is the solute concentration far from the interface, γ is the surface tension, L_v is the latent heat per unit volume, T_M is the melting temperature of the pure material, and k is the segregation coefficient. The equilibrium melting temperature of a dilute binary alloy T is given by

$$T=T_M+mC^*, \tag{4}$$

where m is the slope of the liquidus line in the phase diagram, C^* is the dimensional concentration. The scaled concentration in (1)–(3) is related to the dimensional one by the formula

$$C=\frac{C^*-c_\infty/k}{c_\infty(k-1)/k},$$

and the scaled curvature for a given interface shape $h(x,y,t)$ is

$$\mathcal{K}(h)=\frac{(1+h_x^2)h_{yy}-2h_xh_yh_{xy}+(1+h_y^2)h_{xx}}{(1+h_x^2+h_y^2)^{3/2}}.$$

Boundary condition (2) represents the conservation of solute at the interface, Eq. (3) comes from the conditions of constitutional undercooling [Eq. (4)] and the Gibbs-Thomson effect [1]. To complete the formulation the far-field and sidewall boundary conditions are specified as follows:

$$C\to 1,\quad z\to\infty, \tag{5}$$

$$C_y=0\quad y=\pm d, \tag{6}$$

$$h_y=\pm\cot\phi\quad y=\mp d. \tag{7}$$

Here $2d$ is the thickness of the Hele-Shaw cell in units of δ_c.

In deriving a long-wave evolution equation Riley and Davis [7] are followed and one considers the limit of small segregation coefficient and large surface energy. Let us define

$$\varepsilon\equiv\Gamma^{-1/2}$$

and rescale the system as follows:

$$\varepsilon(x,y)=(X,Y),\quad \varepsilon^2 t=T,$$

$$\varepsilon^{-2}k=\kappa,\quad h(x,y,t)=H(X,Y,T).$$

It is important to note that the assumption about the length scale in the y direction relies on the fact that the interface shape is a slowly varying function of y as suggested by a previous analytical study [5]; this has to be checked *a posteriori*.

We follow Riley and Davis and write the leading-order concentration profile in the form

$$C=1-A(X,Y,T)e^{H-z},$$

where

$$A(X,Y,T)=1-M^{-1}H+\nabla^2H.$$

This has to satisfy the no-flux boundary condition at the side walls (6). The straightforward differentiation of the equation for C leads to the following boundary condition:

$$(\nabla^2H)_Y=(M^{-1}-1+M^{-1}H-\nabla^2H)H_Y,\quad Y=\pm D. \tag{8}$$

Here the rescaled half-thickness of the Hele-Shaw cell is defined as $D=\varepsilon d$. The second boundary condition follows immediately from (7) and can be written in the form

$$\varepsilon H_Y=\pm\cot\phi,\quad Y=\mp D. \tag{9}$$

The long-wave equation is then derived by exactly the same procedure as for infinite domain [7]; the result is

$$H_T-M\nabla^2H_T+M\nabla^4H+\delta\nabla^2H+\kappa H =\nabla\cdot(H\nabla H)-M\nabla\cdot(\nabla^2H\nabla H), \tag{10}$$

where $\delta=M-1-\kappa M$. Thus, the equation obtained here is identical to that of Riley and Davis [7]; the boundary conditions, however, are different. This system could now be solved numerically, but first use is made of analytical methods.

III. ANALYTICAL RESULTS

A. Basic state and linear stability

Let us assume that the contact angle ϕ is close to $\pi/2$,

$$\phi=\frac{\pi}{2}-p\varepsilon, \quad \varepsilon\ll p\ll 1,$$

and use a perturbation expansion in powers of p to determine the x-independent basic-state interface,

$$H_B=pH_1+p^2H_2+\cdots.$$

The basic-state interface shape is the function of y only and can be expressed in terms of the Fourier series as

$$H_B=\sum_{n=0}^{\infty} H_B^{(n)}\cos a_nY, \quad a_n=\frac{\pi n}{D},$$

where the Fourier coefficients can also be expanded in powers of p:

$$H_B^{(n)}=pH_1^{(n)}+p^2H_2^{(n)}+\cdots.$$

The coefficients of the series expansion of the leading-order solution, $H_1^{(n)}$, are found from the two-dimensional version of the long-wave evolution equation, which can be written in Fourier space as

$$M(H_{1YYYY})_n+\delta(H_{1YY})_n+\kappa H_1^{(n)}=0, \quad n=1,2,\ldots. \tag{11}$$

Here only the leading-order terms in powers of p are considered. Integration by parts can be used to obtain the following expression for the Fourier component of the second derivative:

$$(H_{1YY})_n\equiv\frac{1}{D}\int_{-D}^{D}H_{1YY}\cos a_nY\,dY$$
$$=2D^{-1}(-1)^{n+1}-a_n^2H_1^{(n)}, \tag{12}$$

where the contact-angle condition (9) has been used. A similar expression can be obtained for the Fourier component of the fourth derivative by using the linearized version of the boundary condition (8) combined with Eq. (9),

$$(H_{1YYYY})_n=2D^{-1}(-1)^{n+1}(M^{-1}-1-a_n^2)+a_n^4H_1^{(n)}. \tag{13}$$

After substituting the expressions (12) and (13) into Eq. (11) the following formula is obtained for the leading-order Fourier components of the basic state:

$$H_1^{(0)}=-\frac{M}{D},$$

$$H_1^{(n)}=2MD^{-1}(-1)^n\frac{\kappa+a_n^2}{\delta a_n^2-Ma_n^4-\kappa}, \quad n=1,2,\ldots. \tag{14}$$

A similar approach can be used to calculate the higher-order terms. Let us now consider its stability by studying the time evolution of a small disturbance of the form

$$H'=\tilde{\varepsilon}u(X,Y,T), \quad \tilde{\varepsilon}\ll p\ll 1,$$

where $\tilde{\varepsilon}$ is the disturbance amplitude, independent of parameter ε. At neutral stability ($u_T=0$) the function u satisfies the following system:

$$M\nabla^4u+\delta\nabla^2u+\kappa u=\nabla\cdot(H_B\nabla u+u\nabla H_B)$$
$$-M\nabla\cdot(\nabla^2u\nabla H_B+\nabla^2H_B\nabla u), \tag{15}$$

$$u_Y=0, \quad Y=\pm D, \tag{16}$$

$$(\nabla^2u)_Y=(M^{-1}u-\nabla^2u)(\pm p), \quad Y=\mp D, \tag{17}$$

where now $\nabla=(\partial_X,\partial_Y)$. Note that for planar front ($p=0$) the eigenfunctions are simply sines and cosines, and the characteristic equation at the neutral stability condition reduces to

$$M|\mathbf{a}|^4-\delta|\mathbf{a}|^2+\kappa=0.$$

Here $\mathbf{a}$ is the wave vector of the disturbance [7]. The critical values of $|\mathbf{a}|^2$ and the scaled segregation coefficient are given by

$$\kappa_c=(M^{1/2}-1)^2/M, \quad a_c^2=(M^{1/2}-1)/M. \tag{18}$$

If the thickness $2D$ is smaller than $\frac{1}{2}\lambda=\pi/a_c$, one-half of the critical wavelength λ, then the critical disturbance is independent of Y; for larger values of the thickness three-dimensional structures can develop from the planar interface. Both cases are relevant experimentally.

For small values of the contact-angle parameter p the shape of the interfacial disturbance can be written as the following asymptotic expansion:

$$u=u_0+pu_1+p^2u_2+\cdots, \tag{19}$$

where the leading-order term u_0 is the eigenfunction of the stability problem for planar interface. Let us first assume that the thickness is smaller than the resonant value π/a_c such that both D and $4D-\lambda$ are $O(1)$ quantities. Then the leading-order disturbance can be written in the form

$$u_0=u_0^{(0)}e^{iaX}+\text{c.c.}$$

and the above asymptotic expansion for u in powers of the contact-angle parameter is uniformly valid. Here ''c.c.'' denotes complex conjugate. The stability for near-resonant values of thickness will be discussed later in this subsection.

Let us write the Fourier expansion for the first-order solution in the form

$$u_1=e^{iaX}\sum_{n=0}^{\infty}u_1^{(n)}\cos(a_nY), \quad a_n=\frac{\pi n}{D},$$

substitute this expansion into the system (15)–(17), and collect all terms at $O(\tilde{\varepsilon}p)$; this gives expressions for the Fourier coefficients at this order in the form:

$$u_1^{(n)}=u_0^{(0)}\frac{2Ma^2D^{-1}(-1)^{n+1}-(a^2+a_n^2+2Ma^2a_n^2)H_1^{(n)}}{M(a^4+2a^2a_n^2+a_n^4)-\delta(a^2+a_n^2)+\kappa},$$

$$u_1^{(0)}=0.$$

The perturbation problem has a unique solution only when the scaled segregation coefficient κ is equal to κ_c; thus no correction to the stability boundary is found at this order. The asymptotic expansion of κ therefore takes the form:

$$\kappa=\kappa_c+p^2\kappa_2+\cdots.$$

There is no first-order correction to the wave number as well. At the second order in p it is sufficient to integrate the equation for u_2 to see that a solvability condition must be satisfied in order for solution to exist. This leads to an expression for κ_2 in the form

$$\kappa_2=\frac{e^{-iaX}}{2Du_0^{(0)}(1+Ma^2)}\int_{-D}^{D}u_{1XX}(H_1-MH_{1YY})dY.$$

This can be expressed in terms of the known Fourier coefficients

$$\kappa_2=\sum_{n=1}^{\infty}\frac{a^2[2Ma^2D^{-1}(-1)^{n+1}-(a^2+a_n^2+2Ma^2a_n^2)H_1^{(n)}][2MD^{-1}(-1)^{n+1}-(1+Ma_n^2)H_1^{(n)}]}{2[M(a^4+2(aa_n)^2+a_n^4)-\delta(a^2+a_n^2)+\kappa_c](1+Ma^2)}.$$

The correction to the critical value of κ is plotted as a function of the morphological number in Fig. 2, together with corresponding results for the infinite domain [7]. Clearly the effect is destabilizing for all values of the morphological number. This is consistent with the experimental observations [2] and other solidification models [4,5].

Let us now turn to the resonant case. First assume that thickness $2D$ is exactly equal to π/a_c and study the stability of the interface with respect to the antisymmetric disturbances. Those give $O(p)$ corrections to the stability criterion, while symmetric ones only contribute at the second order, as discussed above. A Fourier expansion for an arbitrary odd function of Y can be written as

$$u=\sum_{n=1}^{\infty}v^{(n)}\sin(\alpha_nY),\quad \alpha_n=\pi n/2D. \tag{20}$$

The function u still satisfies the same general stability problem (15)–(17). In the calculation below the subscript ''c'' is dropped; the wave number is fixed and is equal to the critical value appropriate to the boundary condition.

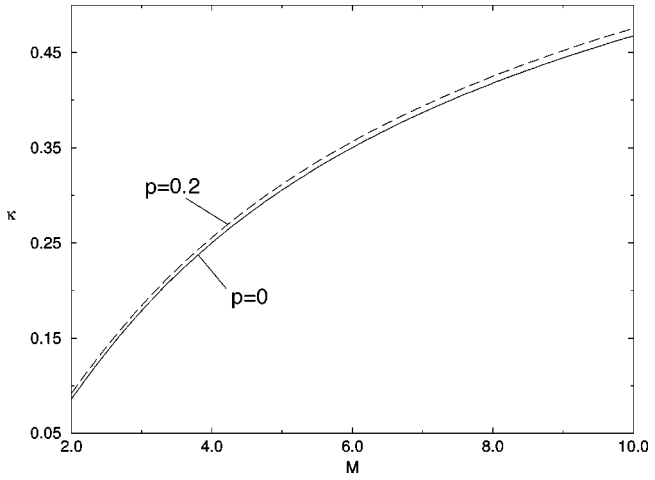

FIG. 2. Neutral stability curve for a nonplanar solidification front obtained from the leading-order perturbation theory (dashed line) for $p=0.3$. The value of thickness is $D=\lambda/8$. Solid lines represent stability boundaries for the same equation on the infinite domain.

Both the numerical solution and the structure of analytical expressions below suggest that the Fourier coefficients rapidly decay as n is increased, so it is usually sufficient to consider a two-mode truncation of the series.

The solvability condition is now obtained in the form

$$\kappa-\kappa_c=\frac{a^2}{v^{(1)}\sqrt{M}}[M(H_{BY}u_Y)_1-(H_Bu)_1]. \tag{21}$$

The leading-order terms here are first order in p; if all higher-order contributions are neglected, the values of the correction can be written in the form

$$\kappa-\kappa_c=-\frac{a^2p}{\sqrt{M}}[Ma^2H_1^{(1)}+H_1^{(0)}-\tfrac{1}{2}H_1^{(1)}].$$

Let us now substitute herein the expression for the Fourier coefficients of the basic state and simplify the resulting formula by using the characteristic equation for stability of the planar interface. The result is

$$\kappa-\kappa_c=\frac{2p}{9D\sqrt{M}}(2+Ma^2-M^2a^4). \tag{22}$$

This correction is plotted in Fig. 3 as a function of the control parameter M for $p=0.2$, where a relatively large value of p is considered for the purpose of clarity. The effect is more significant since it is linear in p. Note that positive values of p correspond to the more physically common concave-down interface. If the interface is concave down, the perturbation theory predicts that the effect is destabilizing over a wide range of M. The stabilizing influence for large M may only be suggestive since in the derivation of the equation, M is order one. We note that the conclusion about the destabilizing effect is consistent with a previous result for a different model of solidification [5]. In experiments for near-resonant conditions the effect is also found to be destabilizing for concave-down interfaces [2].

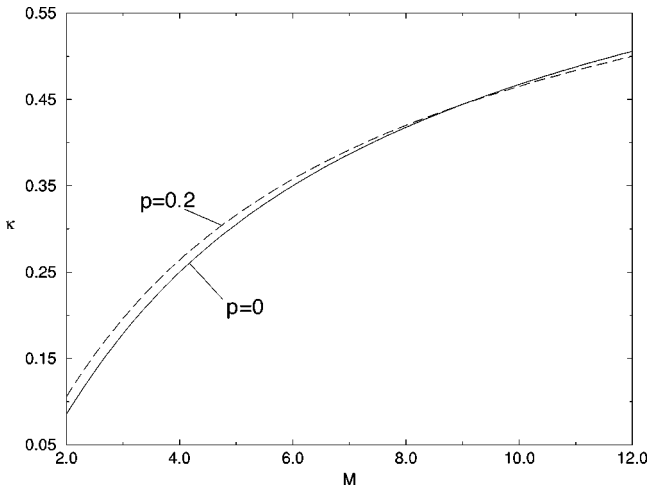

FIG. 3. Neutral stability curves for $p=0.2$, resonant case (dashed line). The value of thickness is $D=\lambda/4$. Solid lines represent stability boundaries for the equation on the infinite domain.

It is important to note that a significant correction to the stability criterion is obtained not only at one special value of thickness, but in a neighborhood of such values. This can be understood from the physical mechanism, which implies resonant-type interaction between the symmetric Fourier mode of steady state and the leading mode of instability; clearly they occur not only for the critical wavelength. Moreover, higher-order resonances can occur for larger values of thickness, when several leading-order wavelengths can fit into the gap. It is clear that such effects can significantly influence pattern formation in the system. This is discussed in the next subsection. For computational simplicity it is assumed that the condition of exact resonance holds; results are qualitatively the same for the near-resonant condition. Also note that patterns for a small nonresonant value of thickness are not discussed in this section; this case, as well as many numerical results for the resonant case, are described in Sec. IV.

B. Weakly nonlinear analysis

Let us reintroduce the small parameter $\tilde{\varepsilon}$ which measures the amplitude of small perturbations and write the asymptotic expansion in the form

$$H=\sum_{i=0}^{\infty}\sum_{j=0}^{\infty}H_{ij}p^i\tilde{\varepsilon}^j.$$

Near the neutral stability curve (for values of the scaled segregation coefficient given by $\kappa(\tilde{\varepsilon})=\kappa-\mu\tilde{\varepsilon}^2$) the nonlinear evolution of the disturbances occurs on a slow time scale $T=\tilde{\varepsilon}^2 t$ [7]. Then, the first-order solution can be written in the form

$$H_{01}=Ae^{iaX}+Be^{iaY}+\text{c.c.} \tag{23}$$

Here c.c. denotes complex conjugate. Let us introduce the linear operator

$$\mathcal{L}\equiv M\nabla^4+\delta\nabla^2+\kappa.$$

At the second order in $\tilde{\varepsilon}$ one obtains the following problem [here it is assumed that $O(\tilde{\varepsilon}^2)$ is not coupled to any terms that depend on p]:

$$\mathcal{L}H_{02}=\frac{1}{2}\nabla^2H_{01}^2-M\nabla\cdot(\nabla^2H_{01}\nabla H_{01}). \tag{24}$$

Further calculation can be simplified if one uses the following easily verified identity:

$$\nabla^2H_{01}=-a^2H_{01}.$$

In particular, it allows us to simplify the right-hand side of Eq. (24) so that the $O(\tilde{\varepsilon}^2)$ problem becomes

$$\mathcal{L}H_{02}=\frac{1+a^2M}{2}\nabla^2H_{01}^2.$$

No solvability condition arises at this order; the solution is found by applying the inverse operator $\mathcal{L}^{-1}$ to the right-hand side of the last equation and substituting the expression (23) for H_{01} in terms of the amplitudes A and B into its right-hand side, which yields

$$H_{02}=-\xi(\tfrac{1}{9}A^2e^{2iaX}+\tfrac{1}{9}B^2e^{2iaY}-ABe^{iaX+iaY}-AB^*e^{iaX-iaY}+\text{c.c.}),$$

where $\xi=2M^{-1}(a^2M+1)/a^2$. At the order of $\tilde{\varepsilon}^3$ one obtains the following problem:

$$\mathcal{L}H_{03}=\mu H_{01}+\nabla^2(H_{01}H_{02})-M\nabla\cdot(U_{01}\nabla H_{02}+U_{02}\nabla H_{01}). \tag{25}$$

Here and in all subsequent calculations the functions U_{ij} are defined for all integer values of i and j according to $U_{ij}=\nabla^2H_{ij}$.

There are secular terms of the type e^{iaX} and e^{iaY} on the right-hand side of Eq. (25); the solvability condition requires that

$$A_T=\mu A-\alpha_0|A|^2A-\beta_0|B|^2A,$$

$$B_T=\mu B-\alpha_0|B|^2B-\beta_0|A|^2B,$$

where the constants α_0 and β_0 are given by the following expressions:

$$\alpha_0=\frac{2(2\sqrt{M}-3)}{9M},\quad \beta_0=\frac{4(\sqrt{M}-2)}{M}. \tag{26}$$

The region of subcritical bifurcation corresponds to negative values of α_0, and the transition point ($\alpha_0=0$) is at $M=9/4$. There are two types of steady-state solutions: two-dimensional cells (either $A=0$ or $B=0$) and square-type pattern, for which the two amplitudes are equal ($A=B$). Two-dimensional cells are stable if

$$1-\frac{\beta_0}{\alpha_0}<0.$$

Nonsecular terms on the right-hand side of Eq. (25) also contribute to the $O(\tilde{\varepsilon}^3)$ solution, which can be written in the form

$$H_{03}=\mathcal{H}B^3e^{3iaY}+\mathcal{H}_1Ae^{iaX}(B^2e^{2iaY}+B^{*2}e^{-2iaY})+\text{c.c.}+\cdots, \tag{27}$$

$$\mathcal{H}=\frac{-\xi a^2(1+2Ma^2)}{81Ma^4-9\delta a^2+\kappa_c},\quad \mathcal{H}_1=\frac{\xi a^2(40-55Ma^2)}{9(25Ma^4-5\delta a^2+\kappa_c)}. \tag{28}$$

Here we give explicit expressions only for those terms which contribute to the contact-angle corrections calculated below.

Let us now discuss changes in the bifurcation structure due to the contact-angle effects (nonzero values of p). The $O(\tilde{\varepsilon}p)$ problem is formulated as follows:

$$\mathcal{L}H_{11}=\nabla^2(H_{01}H_{10})-M\nabla\cdot(U_{01}\nabla H_{10}+U_{10}\nabla H_{01}).$$

The solvability condition at this order gives corrections to the stability criterion, as discussed in Sec. III B. There are also nonsecular terms on the right-hand side; corresponding terms in the solution are found by using the inverse of the linear operator $\mathcal{L}$ and known expressions for H_{10} and H_{01}. The result can be written as follows:

$$H_{11}=\hat{H}Be^{3iaY}+\hat{H}_1e^{2iaY}(Ae^{iaX}+A^*e^{-iaX})+\text{c.c.},$$

$$\hat{H}_1=-\frac{a^2H_B^{(1)}(5+6Ma^2)}{2(25Ma^4+5\delta a^2+\kappa)},\quad \hat{H}=\frac{9(H_B^{(1)}-2H_B^{(2)}Ma^2)}{81Ma^4+9\delta a^2+\kappa}.$$

At the second order in $\tilde{\varepsilon}$ the contact-angle corrections are found from the following system:

$$\mathcal{L}H_{12}=\nabla^2(H_{01}H_{11}+H_{10}H_{02})-M\nabla\cdot(U_{01}\nabla H_{11}+U_{11}\nabla H_{01}+U_{10}\nabla H_{02}+U_{02}\nabla H_{10}).$$

Solvability condition at this order is satisfied automatically [9]; solution terms required at the next order are given by

$$H_{12}=K_1e^{2iaY}+(AB^*e^{iaX}+A^*B^*e^{-iaX})Ke^{iaY}+\text{c.c.}, \tag{29}$$

where

$$K_1=-\frac{1}{9a^2M}\left[\xi H_B^{(2)}B^{*2}\left(\frac{2}{9}+\frac{16Ma^2}{3}\right)+8|A|^2\hat{H}_1\sqrt{M}\right],$$

$$K=\frac{\xi H_B^{(1)}(2\sqrt{M}-1)-\hat{H}_1(\sqrt{M}+1)}{a^2M}.$$

At the $O(p\tilde{\varepsilon}^3)$ the right-hand side contains secular terms of the form

$$-a^2(\mathcal{R}_1-Ma^2\mathcal{R}_2)e^{iaX}-a^2(\mathcal{S}_1-Ma^2\mathcal{S}_2)e^{iaY}+\text{c.c.},$$

where

$$\mathcal{R}_1=\left(\frac{\xi\hat{H}_1}{9}+\mathcal{H}_1H_B^{(1)}+K\right)[(B^*)^2+B^2]A,$$

$$\mathcal{S}_1=\xi\left(\tfrac{1}{9}\hat{H}|B|^2B^*-2|A|^2B^*\hat{H}_1\right)+\tfrac{1}{2}\mathcal{H}(H_B^{(1)}B^3+H_B^{(2)}B^{*3})+2|A|^2B^*K+B^*K_1,$$

$$\mathcal{R}_2=\left(\frac{4\xi}{9}\hat{H}_1+2\mathcal{H}_1H_B^{(1)}+K\right)(B^{*2}+B^2)A,$$

$$\mathcal{S}_2=\xi\left(2\hat{H}_1|A|^2B^*+\tfrac{10}{3}\hat{H}B^{*2}B\right)+\mathcal{H}(6H_B^{(1)}B^3-24H_B^{(2)}B^{*3}-9H_B^{(1)}B^{*3}+18H_B^{(2)}B^3)-2K_1B^*+2|A|^2B^*K.$$

In order to eliminate these secular terms a solvability condition has to be satisfied, which is written in the form

$$A_T=\mu A-\alpha_0|A|^2A-\beta_0|B|^2A-\frac{a^2p}{\sqrt{M}}(\mathcal{R}_1-Ma^2\mathcal{R}_2),$$

$$B_T=\mu B-\alpha_0|B|^2B-\beta_0|A|^2B-\frac{a^2p}{\sqrt{M}}(\mathcal{S}_1-Ma^2\mathcal{S}_2).$$

These conditions can also be interpreted in terms of corrections to the coefficients α_0 and β_0 [9]. This approach yields a modified system of amplitude equations in the form:

$$A_T=\mu A-\alpha_0|A|^2A-\beta B^2A,$$

$$B_T=\mu B-\alpha B^3-\beta_0|A|^2B,$$

where

$$\alpha=\alpha_0+p\alpha_1+\cdots,\quad \beta=\beta_0+p\beta_1+\cdots.$$

The no-flux boundary condition requires the amplitude B to be purely imaginary. For planar front steady-state cellular structures can be observed near the bifurcation point in the region of parameters where the initial bifurcation is supercritical. Both the amplitude of such cells and the location of the transition point between the regions of supercritical and subcritical bifurcations will change due to the contact angle. For positive p the region of subcritical bifurcation is expanded, as shown in Fig. 4. The changes in the bifurcation structure are illustrated in Fig. 5—they are similar to those found in [5]. Stable two-dimensional structures with $B=0$ correspond to interfaces which are symmetric with respect to the center plane.

For the values of control parameter $\kappa(\tilde{\varepsilon})=\kappa-\mu\tilde{\varepsilon}^2$ the interface may be unstable with respect to modulations—disturbances of the larger scale $\hat{X}=\tilde{\varepsilon}^2X$. In an infinite three-dimensional system there is an annular ring of the unstable wave numbers for this modulational instability [13], the thickness of the ring is $O(\tilde{\varepsilon}^2)$, see Fig. 6. For the Hele-Shaw cell the system is essentially two dimensional for small enough values of thickness when no wave numbers with a nonzero y-component are allowed. If the thickness is now increased to the point when there is only one admissible value of this component (dashed line in Fig. 6), then the weakly nonlinear analysis will lead to the following system of amplitude equations:

$$A_T=\mu A-\alpha_0|A|^2A-\beta B^2A+\gamma\frac{\partial^2A}{\partial\hat{X}^2},$$

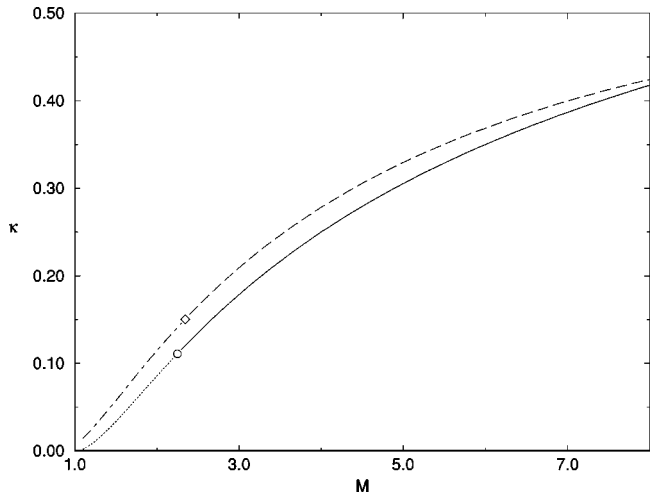

FIG. 4. Location of the transition point on the neutral stability curve for the resonant case. Solid and dotted lines denote the regions of supercritical and subcritical bifurcations, respectively, for the two-dimensional case ($p=0$). For $p=0.1$ the supercritical bifurcation corresponds to the dashed line, the subcritical bifurcation to the dash-dotted line.

$$B_T=\mu B-\alpha B^3-\beta_0|A|^2B.$$

Notice that modulational terms are present only for A. In order to find the value of the coefficient γ we expand the linear operator in powers of $\tilde{\varepsilon}$:

$$\mathcal{L}=\mathcal{L}_0+\tilde{\varepsilon}\mathcal{L}_1+\cdots,$$

and then substitute this into all terms of the equation, including nonlinear ones. At the second order in $\tilde{\varepsilon}$ there is no additional contribution due to the contact angle, but solvability condition at the third order gives corrections to the value of γ [9].

Since the value of γ now depends on the contact angle, the modulational stability boundary is different. The results are shown in Fig. 7; the domain of modulational instability is expanded.

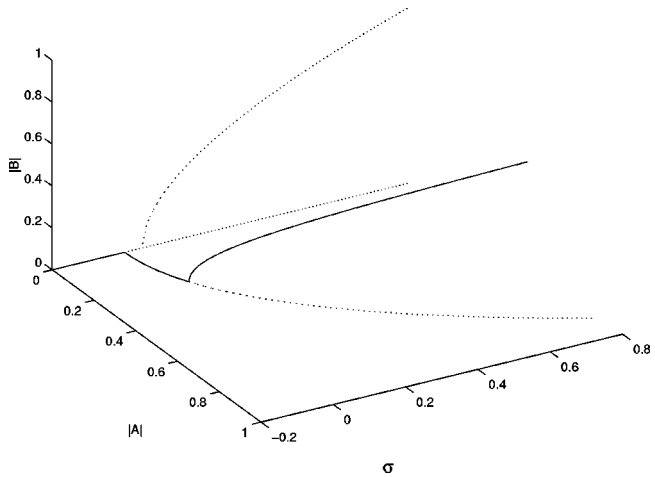

FIG. 5. Bifurcation diagram for nonzero values of p for the resonant case. Absolute values of the amplitudes in both directions are plotted versus the control parameter. Dotted lines denote unstable branches. The primary bifurcation is centerline symmetric, the secondary is centerline antisymmetric, and the secondary bifurcation point approaches the primary as $p\to 0$.

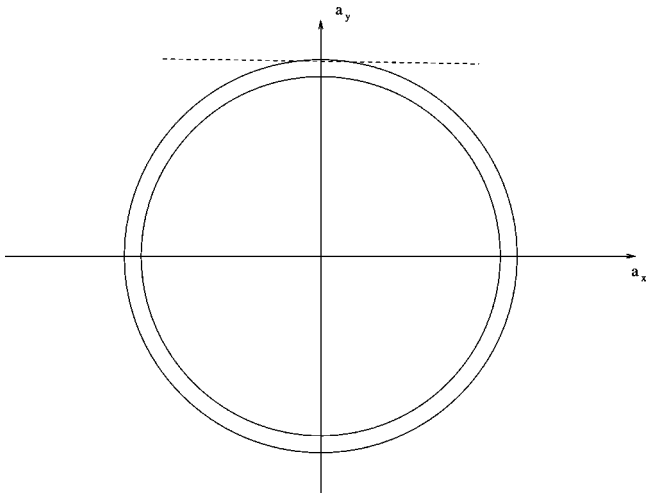

FIG. 6. Unstable wave numbers for modulations in three dimensions (inside the annular ring). Only two values of the y component are allowed for the Hele-Shaw case.

IV. NUMERICAL SOLUTION

In order to check the analytical results and study strongly nonlinear evolution of the solidification front the long-wave evolution equation (10) is solved numerically with the boundary conditions (8) and (9) and periodic boundary conditions in the X direction. Spatial discretization is performed using finite differences on a uniform mesh in the Y direction and Fourier components in the X direction. The grid points at the boundaries $Y=-D$ and $Y=D$ require special treatment. For a fixed value of X the function $H(X,Y)$ at the two grid points adjacent to each of the walls can be expressed as a Taylor series about the end points. The first and third derivatives are eliminated from such expressions by using the boundary conditions (8) and (9). Then each Taylor expansion is truncated to the fourth order, which leads to a linear system of two equations for the unknown second and fourth derivatives at each end. After this system is solved, all derivatives in the fourth-order Taylor expansions about the end points are known: we use these expansions to extrapolate the

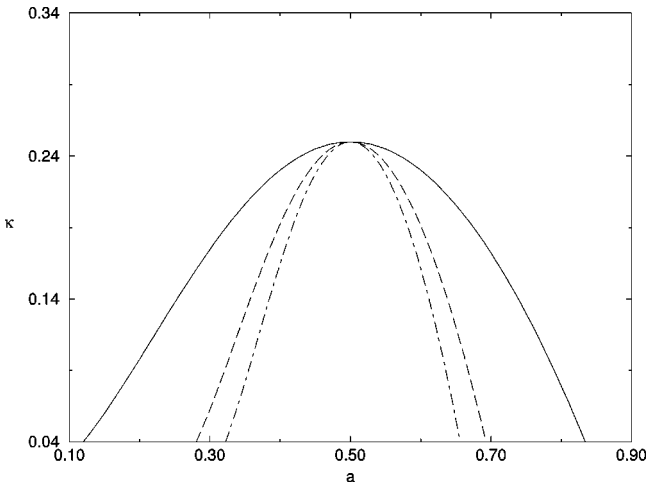

FIG. 7. Corrections to the modulational stability boundary. The solid line represents the linear stability curve, the dashed line represents the Eckhaus curve, and the dash-dotted line is the modulational stability boundary for $p=0.03$.

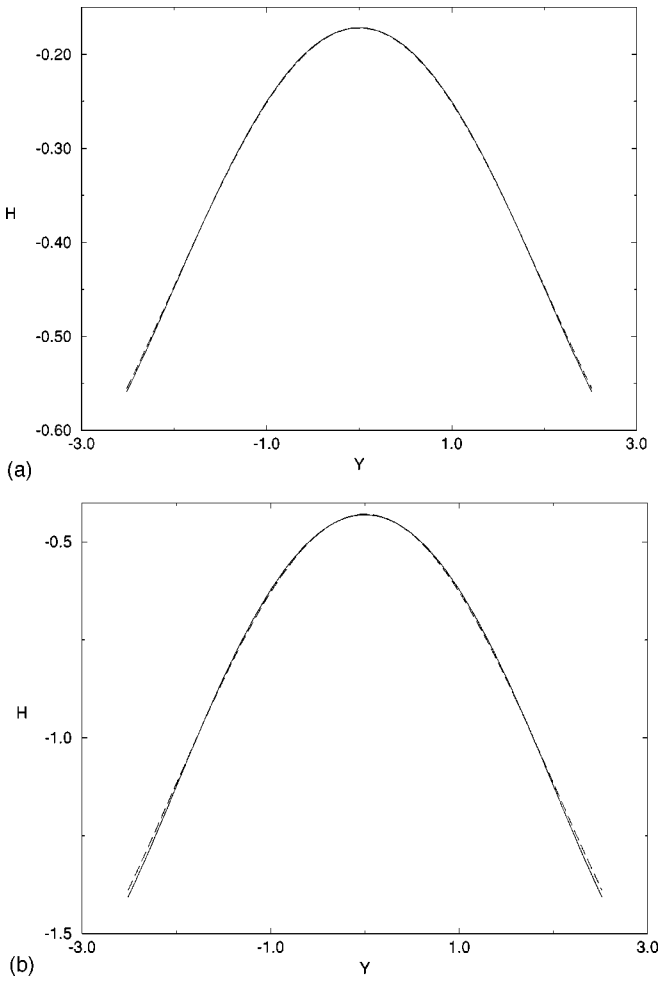

FIG. 8. Steady-state interface shapes obtained numerically for $M=4.0, \kappa=0.25, D=0.2\lambda$ (solid lines). Dashed lines represent perturbation theory results. The values of the contact-angle parameter are $p=0.2$ (a) and $p=0.5$ (b).

function outside its physical domain of definition. Now all spatial derivatives can be evaluated by standard central-difference formulas. Time-stepping is performed by Gear's method (backward differentiation formulas) using standard subroutines from the *IMSL* software package.

At sufficiently small values of thickness and length in the X direction, for which the curved-front solution should be stable according to the analytical formulas from the preceding section, the numerical solution quickly approaches steady state. This one-dimensional numerical interface shape was compared to the perturbation solution given by Eq. (14). The numerical steady-state solutions are shown in Fig. 8 together with the perturbation theory results (dashed lines). Clearly they are in a very good agreement even for relatively large values of p: interface shapes are almost identical for $p<0.1$ and only small error can be seen for larger values of the parameter [such as $p=0.5$, Fig. 8(b)].

Let us now increase the value of thickness to the point where asymmetric disturbances can grow. Consider the range of parameters where bifurcation in the unperturbed system is supercritical. For relatively small values of p the front quickly approaches the symmetric state, then after some time the instability develops which leads to asymmetric steady-state structure similar to finite-amplitude solution of the unperturbed problem. The stability boundary can be found numerically and then compared to linear theory. For small values of $p<0.01$ the leading-order perturbation theory result (22) is in very good agreement with the numerics; for larger values of p it becomes inaccurate despite the fact that basic state is still well represented by the perturbation approximation. The error in linear stability is due to inaccurate representation of the eigenfunction u. If one uses a two-mode truncation in the Fourier expansion of u, the agreement becomes much better. This can be seen in Fig. 9: the solid line represents formula (21), the dashed line leading-order correction (22); circles correspond to the numerical result.

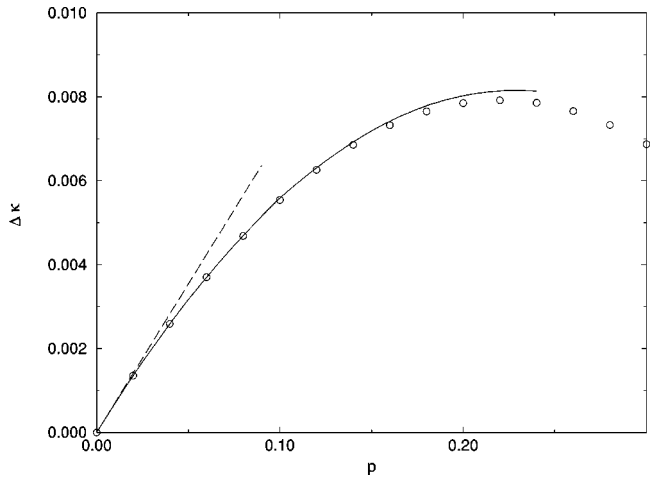

FIG. 9. Linear stability criterion for symmetric interface shapes at $M=4$. Correction to the scaled segregation coefficient, $\Delta\kappa=\kappa-\kappa_c$, is plotted as a function of p for $D\sim 0.5\lambda$. The solid line represents the two-mode Galerkin approximation, the dashed line represents the first-order perturbation solution, and the circles represent the numerical results.

In order to verify the validity of the long-wave approach the derivative with respect to y was calculated for all numerical solutions; it is consistent with the scaling we used, i.e., all solutions are slowly varying functions of y [9]. It is also important to note that the angle between the interface and the wall in the cross section θ is different from the actual contact angle. A simple geometric construction allows one to find the relation between those in the form

$$\tan\theta=\tan\phi/\sqrt{1+H_X^2}.$$

Let us now discuss the fully three-dimensional evolution. First, consider a small value of thickness ($D=\lambda/8$), when steady-state structures in the weakly nonlinear regime are almost two dimensional for small p. In the strongly nonlinear regime two-dimensional cellular structures with deep roots are known to appear in the numerical solutions [10,11]; these simulations are often used to model similar structures in experiments. Experimental results, however, depend on thickness [12], while previous numerical simulations did not take into account three-dimensional effects. It was found from our numerical solution that stable three-dimensional structures exist for a range of values of contact angles and depend on thickness, typical results are shown in Fig. 10(a). The solutions are flattened at the top and thus similar to experimentally observed shallow cells. The interface shapes depend on the contact angle, as is illustrated in Fig. 10(b), where cross

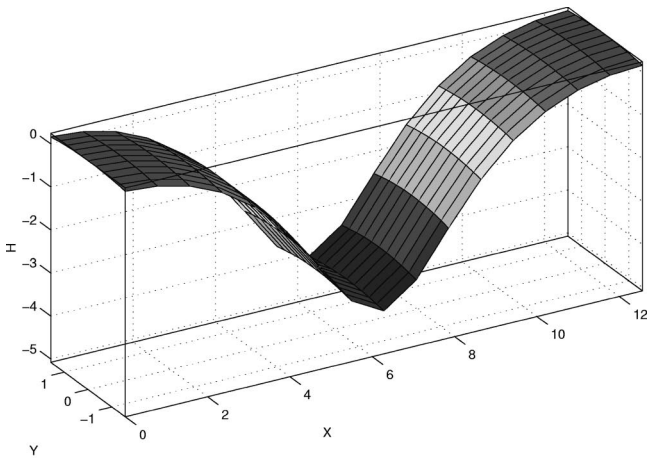

(a)

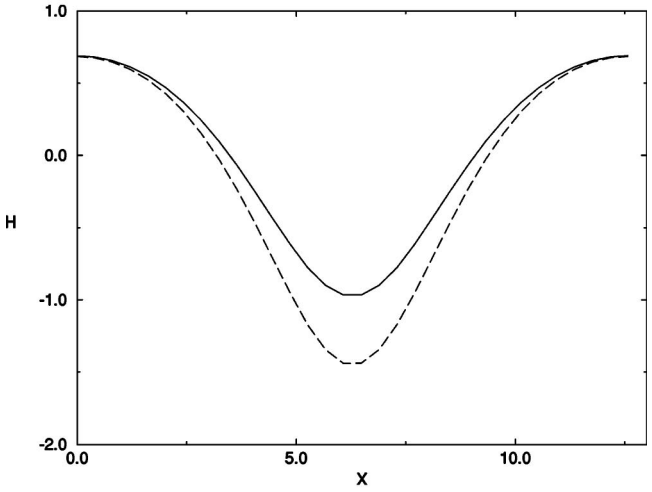

(b)

FIG. 10. Results of numerical simulations for a small value of nondimensional thickness $D=\lambda/8$. (a) Three-dimensional steady-state interface shapes in the strongly nonlinear regime for $\kappa-\kappa_c=0.03$. (b) Cross sections of the front for different values of the contact angle. The solid line corresponds to the two-dimensional problem, the dashed line to the steady-state solution with $p=0.01$.

sections of the interface shapes are shown for the values $p=0$ and 0.01. Characteristic amplitude of the solution is larger due to the presence of three-dimensional effects. Thus, we expect that contact-line effects for concave-down interfaces promote formation of the rootlike structures. Since deep cells typically have smaller spacing, a decrease in spacing can be expected due to three-dimensional effects; this may expain the fact that experimentally observed spacing in cellular structures at low speeds is typically smaller than predicited by two-dimensional models [12]. Careful measurement of the amplitudes of cells is needed to verify this hypothesis. In the region of subcritical bifurcation it was found that the secondary bifurcation to stable solutions can be promoted due to contact-angle effects.

Larger values of thicknesses were also considered, where resonant effects are more important. In the weakly nonlinear regime the main results about competition between two- and three-dimensional patterns were verified numerically. Typical structures in this regime are shown in Fig. 11; they tend to be more unstable than one would expect from the perturbation theory.

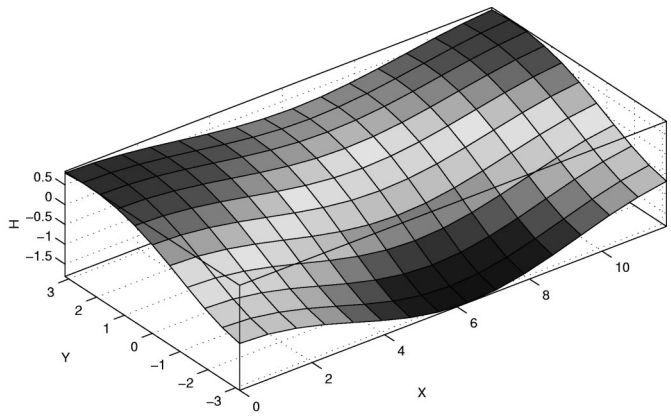

FIG. 11. Interface shapes in the weakly nonlinear regime for a larger value of thickness, $D=\lambda/4$. The interface is no longer symmetric with respect to the center plane.

V. CONCLUSIONS

Three-dimensional effects are considered in directional solidification in Hele-Shaw cells in the limit when the gap width is much larger than the solute diffusion length. The system is described by a long-wave evolution equation subject to appropriate boundary conditions. When the contact angle satisfies $|\phi-\pi/2|\propto p\ll 1$, asymptotic expansions are used to describe the behavior of the interface. At arbitrary values of contact angles the system is solved numerically by a finite difference method.

It is found that for sufficiently small values of the gap thickness the interface always remains symmetric with respect to the center line; for small values of p the asymptotic theory indicates that such a curved front is less stable than planar basic-state solution, the corrections are second order in p and therefore usually small. In the strongly nonlinear regime numerical solutions indicate the appearance of steady-state cellular structures that satisfy the boundary conditions at the walls. Formation of rootlike structures is promoted for concave-down interfaces as p is increased.

As the value of the thickness is increased to approach the one-half of the wavelength of instability, resonant-type nonlinear interactions between the most unstable disturbance and the symmetric basic-state solution determine the behavior of the interface. They lead to destabilization of the concave-down interface; this effect is linear in p. Weakly nonlinear analysis shows that appearance of three-dimensional structures can be delayed; this is also confirmed by numerics. The region of instability due to modulations expands due to the presence of contact-angle effects. Numerical results suggest that for large p interfaces symmetric in Y tend to be more stable than predicted by perturbation theory. In the strongly nonlinear regime fully three-dimensional steady-state solutions are found; the secondary bifurcation to stable solutions is postponed.

ACKNOWLEDGMENTS

This work was supported by a grant from the National Aeronautics and Space Administration, Program on Microgravity Science and Applications. Authors are grateful to Professor A. Bayliss for useful advice on numerical computations.

[1] S. R. Coriell and G. B. McFadden, in *Handbook of Crystal Growth, Vol. 1*, edited by D. T. J. Hurle (Elsevier, New York, 1993), pp. 785–857.
[2] S. de Cheveigné, C. Guthmann, and M. M. Lebrun, J. Phys. (Paris) **47**, 2095 (1986).
[3] K. Brattkus and S. H. Davis, J. Cryst. Growth **91**, 538 (1988).
[4] B. Caroli, C. Caroli, and B. Roulet, J. Cryst. Growth **76**, 31 (1986).
[5] V. S. Ajaev and S. H. Davis, Proc. R. Soc. London, Ser. A **455**, 3589 (1999).
[6] G. I. Sivashinsky, Physica D **8**, 243 (1983).
[7] D. S. Riley and S. H. Davis, SIAM (Soc. Ind. Appl. Math.) J. Appl. Math. **50**, 420 (1990).
[8] K. Brattkus and S. H. Davis, Phys. Rev. B **38**, 11 452 (1988).
[9] V. S. Ajaev, Ph.D. thesis, Northwestern University, Evanston, 1999.
[10] A. C. Skeldon, G. B. McFadden, M. D. Imprey, D. S. Riley, K. A. Cliffe, A. A. Wheeler, and S. H. Davis, Eur. J. Appl. Math. **6**, 639 (1995).
[11] D. S. Sarocka, A. J. Bernoff, and L. F. Rossi, Physica D **127**, 146 (1999).
[12] B. Billia, H. Jamgotchian, and H. Nguyen Thi, J. Cryst. Growth **167**, 265 (1996).
[13] M. C. Cross and P. C. Hohenberg, Rev. Mod. Phys. **65**, 851 (1993).